Data in Brief 000 (2020) 105942

Contents lists available at ScienceDirect

Data in Brief

journal homepage: www.elsevier.com/locate/dib

Data Article

Data on molecular docking of tautomers and enantiomers of ATTAF-1 and ATTAF-2 selectivty to the human/fungal lanosterol-14α-demethylase

Hamid Irannejad[a,b], Saeed Emami[a,b], Hassan Mirzaei[c], Seyedeh Mahdieh Hashemi[a,b,*]

[a] Department of Medicinal Chemistry, Faculty of Pharmacy, Mazandaran University of Medical Sciences, Sari, Iran
[b] Pharmaceutical Sciences Research Center, Mazandaran University of Medical Sciences, Sari, Iran
[c] Ischemic Disorders Research Center, Golestan University of Medical Sciences, Gorgan, Iran

ARTICLE INFO

Article history:
Received 13 June 2020
Accepted 24 June 2020
Available online xxx

Keywords:
Molecular docking
Lanosterol-14α-demethylase
Selectivity
Antifungal

ABSTRACT

The data have been obtained for tautomers and enantiomers of ATTAF-1 and ATTAF-2 that were developed based on antifungal standard drugs with triazole scaffold. These compounds were docked into the human and fungal lanosterol-14α-demethylase. In order to validate the data, 8 standard triazole antifungal drugs (Fluconazole, Itraconazole, Posaconazole, Ravuconazole, Albaconazole, Voriconazole, Isavuconazole and Efinaconazole) were also docked into the human and fungal lanosterol-14α-demethylase. The binding conformations of these molecules and their interactions with lanosterol-14α-demethylase may inform the development of further small molecule lanosterol-14α-demethylase inhibitors with significant selectivity toward this enzyme. The analysis has done on the basis of type of interactions (bond type and distance). The length of the Fe-N coordination bond for (*R*)-N2-ATTAF-1 and (*S*)-N1-ATTAF-2 complexes is obtained 6.36 and 4.19 Å, respectively and about 2 Å in the other tautomer and enantiomer complexes, reflecting the lower basicity of the N-4 atom in the 1,2,4-

DOI of original article: 10.1016/j.imu.2020.100366
* Corresponding author at: Department of Medicinal Chemistry, Faculty of Pharmacy, Mazandaran University of Medical Sciences, Sari, Iran.
E-mail address: hashemi325@gmail.com (S.M. Hashemi).

https://doi.org/10.1016/j.dib.2020.105942

triazole ring of (*R*)-N2-ATTAF-1 and (*S*)-N1-ATTAF-2 in comparison with the N-4 atom in the 1,2,4-triazole ring in other tautomers and enantiomers and supporting higher selectivity of (*R*)-N2-ATTAF-1 and (*S*)-N1-ATTAF-2 towards the target CYP51 enzymes vs. human. Interestingly, we have investigated unfavorable interactions (donor-donor) with TRP239 and MET378 for (*R*)-N2-ATTAF-1 and (*S*)-N1-ATTAF-2, respectively. These unfavorable interactions also have been seen in case of posaconazole and isavuconazole. The data presented in this article are related to the research paper entitled "*In silico* prediction of ATTAF-1 and ATTAF-2 selectivity towards human/fungal lanosterol 14α-demethylase using molecular dynamic simulation and docking approaches".

Specifications table

Subject	Computational and *in silico* Chemistry
Specific subject area	Docking studies
Type of data	Table Figure
How data were acquired	ChemDraw Ultra 8.0 and Molecular docking (AutoDockTools-1. 5. 4)
Data format	Raw Analyzed
Parameters for data collection	The docking of the tautomeric and enantiomeric forms of ATTAF-1 and ATTAF-2 was targeted at a 6 Å radius area that encompassed the heme of lanosterol-14α-demethylase (PDBs: 5JLC, 5V5Z, 3LD6) using bond type and distance and interactions of proteins with the ligands.
Description of data collection	The Proteins were collected from Protein Data Bank (www.rcsb.org). Ligands 3D structures were obtained by using ChemDraw Ultra 8.0 and energy minimized using PM3 force field. The docking was done using AutoDockTools-1. 5. 4. Searching algorithm in docking study was lamarckian genetic algorithm.
Data source location	Institution: Mazandaran University of Medical Sciences City/Town/Region: Sari, Farahabad Country: Iran
Data accessibility	Data is with this article.
Related research article	H. Irannejad, S. Emami, H. Mirzaei, S. M. Hashemi, *In silico* prediction of ATTAF-1 and ATTAF-2 selectivity towards human/fungal lanosterol 14α-demethylase using molecular dynamic simulation and docking approaches, https://doi.org/10.1016/j.imu.2020.100366.

Value of the data

- The lanosterol 14α-demethylase has been identified as a molecular target for the treatment of fungal diseases.
- The modeling data was produced to rationalize the structural necessities for lanosterol 14α-demethylase inhibition.
- The binding conformations of the ATTAF-1 and ATTAF-2, their interactions with human and fungal lanosterol 14α-demethylase and coordination bond distance may inform further studies focused on the development of lanosterol 14α-demethylase inhibitors.
- Novel synthetic analogues with improved bioactivity and minimized side effects can be expanded against this target by using this *in silico* docking data and research time can be minimized significantly.

Table 1
List of targets.

Entry	PDB ID	Resolution (Å)	Description	RMSD (Å)
1	5V5Z	2.9	Structure of CYP51 from the pathogen *Candida albicans* [7]	1.71
2	5JLC	2.4	Structure of CYP51 from the pathogen *Candida glabrata* [7]	1.58
3	3LD6	2.8	Crystal structure of human lanosterol 14alpha-demethylase (CYP51) in complex with ketoconazole [8]	1.04

Table 2
Coordinates of the cubic box used to dock ATTAF-1 and ATTAF-2 to the fungal and human CYP51.

Entry	Side	Coordinate		
		CACYP51	CGCYP51	hCYP51
1	X	−42.490	−40.056	42.287
2	Y	−13.523	74.850	4.969
3	Z	26.334	−23.564	1.219

- This dataset can be useful to model other potent antifungal agents in future and researchers in pharmaceutical chemistry can gain from the data.

1. Data description

Lanosterol-14α-demethylase (CYP51) is found in mycobacteria, fungi, plants, animals and humans. This enzyme is required for biosynthesis of sterol in eukaryotes and is the major target for azole antifungal agents [1,2]. In mammals, lanosterol-14α-demethylase is the enzyme that catalyzes lanosterol to cholesterol conversion, which is necessary to maintain a variety of metabolic functions [3]. An ideal antifungal agent should have minimal effect on human CYP51 enzymes while keeping potent inhibition of fungal enzyme to reduce the side effects [4]. Lanosterol-14α-demethylase consists of an iron protoporphyrin unit in its active site. At the molecular level, N-4 in the 1,2,4-triazole ring selectively coordinates to the lanosterol-14α-demethylase heme iron and cause the prevention of the fungal ergosterol biosynthesis pathway [5]. In order support a medicinal chemistry campaign to develop potent azole antifungal agents with high CYP51 affinity, we have previously synthesized and reported a series of novel fluconazole analogues, with the most promising ones introduced as ATTAF-1 and ATTAF-2 [6] and provided the computational-based docking and MD simulation outputs for all tautomeric and enantiomeric forms of ATTAF-1 and ATTAF-2 plus 8 antifungal standard drugs were docked into the human and fungal lanosterol-14α-demethylase [9]. Here, our studies provide important protein-ligand interaction information for the further development of lanosterol-14α-demethylase inhibitors. In this article Table 1 provides the details about the targets and their description. Table 2 gives the coordinates of the cubic box used to dock ATTAF-1 and ATTAF-2 to the fungal and human CYP51. Table 3 gives the length of the Fe-N coordination bond. Table 4 provides tautomers and enantiomers of ATTAF-1 and ATTAF-2 interactions with fungal and human CYP51. To point to the N-4 coordination with heme iron, 3D interactions of all tautomeric and enantiomeric forms of ATTAF-1 and ATTAF-2 with the target enzymes are shown in the Figs. 1–3. 2D interactions of all tautomeric and enantiomeric forms of ATTAF-1, ATTAF-2 and 8 standard triazole antifungal drugs with the target enzymes are shown in the supplemental file.

2. Experimental design, materials and methods

2.1. Protein selection and preparation

The crystal structures of the selected proteins were retrieved from protein data bank. (PDB database, www.rcsb.org). Protein preparation was done by preprocessing the structures by re-

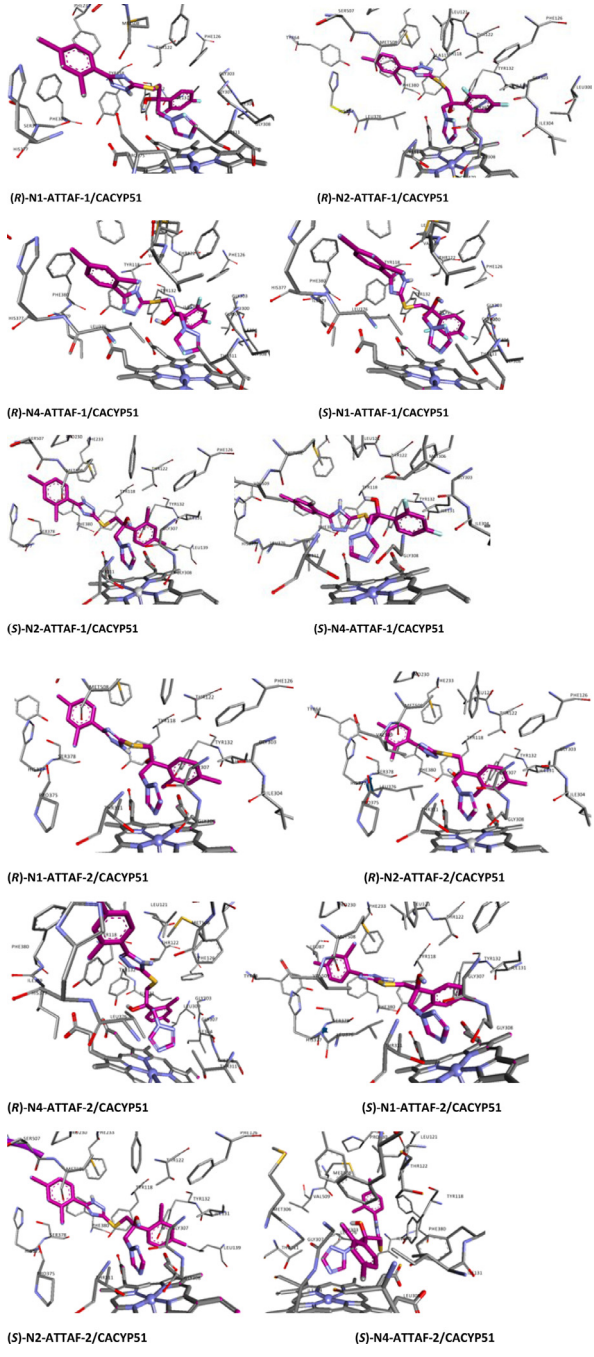

Fig. 1. Ligand interaction map of the predicted binding mode of tautomers and enantiomers of ATTAF-1 and ATTAF-2 in the active site *Candida albicans* CYP51.

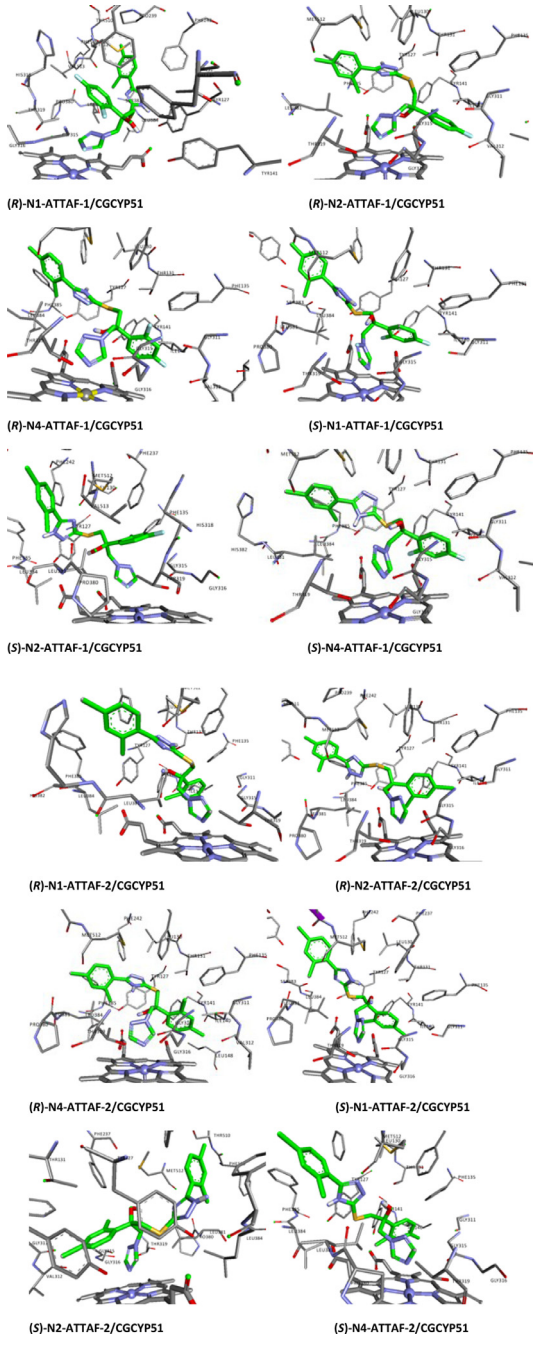

Fig. 2. Ligand interaction map of the predicted binding mode of tautomers and enantiomers of ATTAF-1 and ATTAF-2 in the active site *Candida glabrata* CYP51.

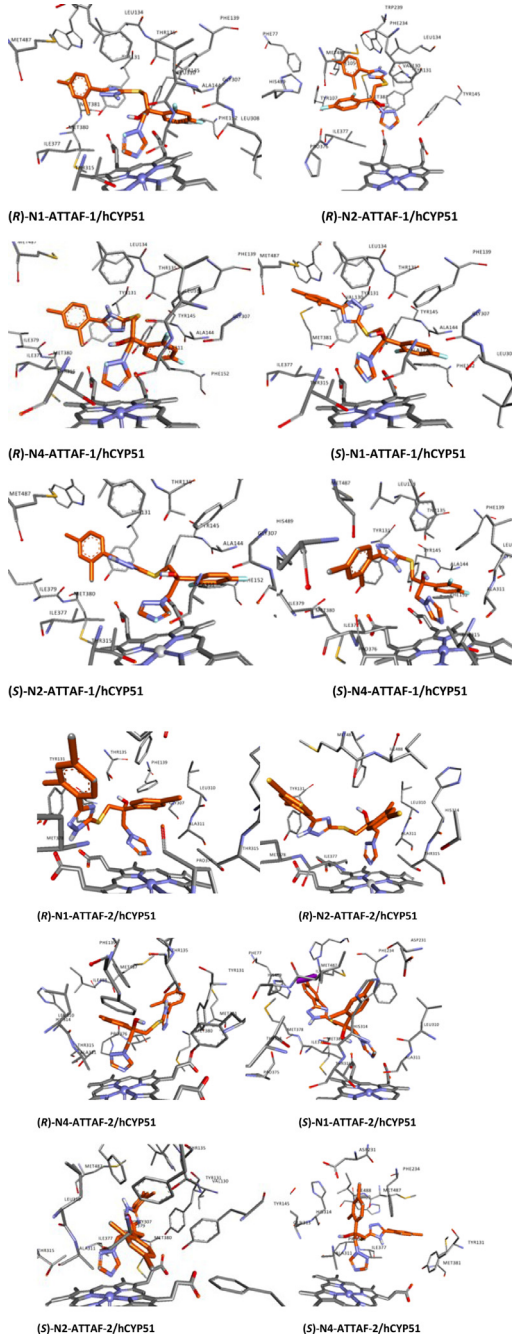

Fig. 3. Ligand interaction map of the predicted binding mode of tautomers and enantiomers of ATTAF-1 and ATTAF-2 in the active site human CYP51.

Table 3
Length of the Fe-N coordination bond.

Entry	Compound	Coordination Bond Distance (Å)		
		CACYP51	CGCYP51	hCYP51
1	(*R*)-N1-ATTAF-1	2.52	2.93	2.17
2	(*R*)-N2-ATTAF-1	2.21	2.63	**6.36**
3	(*R*)-N4-ATTAF-1	2.91	2.25	1.92
4	(*S*)-N1-ATTAF-1	2.56	2.44	2.83
5	(*S*)-N2-ATTAF-1	2.29	2.89	2.92
6	(*S*)-N4-ATTAF-1	2.53	2.80	2.70
7	(*R*)-N1-ATTAF-2	2.32	2.83	2.67
8	(*R*)-N2-ATTAF-2	2.12	2.85	2.19
9	(*R*)-N4-ATTAF-2	2.20	2.26	2.03
10	(*S*)-N1-ATTAF-2	2.33	2.80	**4.19**
11	(*S*)-N2-ATTAF-2	2.45	2.86	2.04
12	(*S*)-N4-ATTAF-2	2.74	2.74	3.12

Table 4
Tautomers and enantiomers of ATTAF-1 and ATTAF-2 interactions with fungal and human CYP51.

Entry	Target	Ligand	Interaction	Type of interaction	Bond distance (Å)
1.	**5V5Z**	(*R*)-N1-ATTAF-1	Tyr132	H-Bond	2.34
			Phe233	Pi-Pi stacking	5.13
			Met508	Pi-Sulfur	5.85
			Tyr118	Pi-Sulfur	3.60
			Phe233	Pi-Sulfur	5.96
		(*R*)-N2-ATTAF-1	Tyr132	H-Bond	2.32
			Phe380	Pi-Pi stacking	4.92
			Met508	Pi-Sulfur	5.45
			Phe228	Pi-Sulfur	5.87
		(*R*)-N4-ATTAF-1	Phe380	Pi-Pi stacking	4.93
			Phe233	Pi-Pi stacking	5.81
			Tyr118	Pi-Pi stacking	3.44
			Ser378	Pi-Pi stacking	4.17
		(*S*)-N1-ATTAF-1	Tyr132	H-Bond	3.16
			Tyr118	Pi-Pi stacking	3.54
			Phe380	Pi-Pi stacking	5.08
		(*S*)-N2-ATTAF-1	Tyr132	H-Bond	3.21
			Tyr118	Pi-Pi stacking	3.71
			Phe380	Pi-Pi stacking	5.91
		(*S*)-N4-ATTAF-1	Ser378	Pi-Pi stacking	4.14
			Phe380	Pi-Pi stacking	4.96
			Phe233	Pi-Pi stacking	5.86
			Tyr118	Pi-Pi stacking	3.52
		(*R*)-N1-ATTAF-2	Phe233	Pi-Pi stacking	5.75
			Phe228	Pi-Sulfur	5.48
		(*R*)-N2-ATTAF-2	Tyr118	Pi-Pi stacking	5.84
			Phe380	Pi-Pi stacking	5.31
		(*R*)-N4-ATTAF-2	Tyr132	H-Bond	2.59
			Tyr118	Pi-Pi stacking	4.45
			Phe228	Pi-Sulfur	5.50
			Met508	Pi-Sulfur	5.41
		(*S*)-N1-ATTAF-2	Phe233	Pi-Pi stacking	5.01
			Tyr118	Pi-Sulfur	4.35
			Met508	Pi-Sulfur	5.62
		(*S*)-N2-ATTAF-2	Tyr118	H-Bond	2.64
			Ser378	H-Bond	2.10
		(*S*)-N4-ATTAF-2	Tyr132	H-Bond	2.94
			Phe380	Pi-Pi stacking	5.93
			Tyr118	Pi-Pi stacking	3.72

(*continued on next page*)

Table 4 (*continued*)

Entry	Target	Ligand	Interaction	Type of interaction	Bond distance (Å)
2.	**5JLC**	(*R*)-N1-ATTAF-1	Tyr127	H-Bond	1.99
			Phe237	Pi-Pi stacking	5.01
		(*R*)-N2-ATTAF-1	Tyr127	Pi-Pi stacking	5.89
			Phe237	Pi-Sulfur	5.02
			Phe135	Pi-Sulfur	5.12
		(*R*)-N4-ATTAF-1	Phe242	Pi-Pi stacking	5.28
			Tyr127	Pi-Pi stacking	5.41
			Phe135	Pi-Pi stacking	5.44
			Tyr141	Pi-Sulfur	5.39
			Met512	Pi-Sulfur	4.82
		(*S*)-N1-ATTAF-1	Tyr141	H-Bond	2.61
		(*S*)-N2-ATTAF-1	His318	H-Bond	2.68
			Thr319	H-Bond	3.58
			Ser383	H-Bond	1.98
			Phe242	Pi-Pi stacking	5.31
			Met512	Pi-Sulfur	5.29
			Tyr127	Pi-Sulfur	4.20
		(*S*)-N4-ATTAF-1	Tyr141	2 H-Bond	2.60, 3.58
			Phe242	Pi-Pi stacking	5.32
			Tyr127	Pi-Pi stacking	4.04
			Tyr141	Pi-Sulfur	4.86
			Tyr127	Pi-Sulfur	3.93
			Met512	Pi-Sulfur	4.79
		(*R*)-N1-ATTAF-2	Tyr141	Pi-Pi stacking	5.42
		(*R*)-N2-ATTAF-2	Ser383	H-Bond	2.09
			Phe385	Pi-Pi stacking	5.01
			Met512	Pi-Sulfur	4.93
		(*R*)-N4-ATTAF-2	Tyr141	Pi-Sulfur	5.10
			Phe237	Pi-Sulfur	5.80
		(*S*)-N1-ATTAF-2	Phe242	Pi-Pi stacking	5.54
			Phe385	Pi-Pi stacking	5.89
			His382	Pi-Pi stacking	5.31
			Tyr127	Pi-Sulfur	4.16
			Met512	Pi-Sulfur	5.46
		(*S*)-N2-ATTAF-2	Tyr127	H-Bond	2.86
			Ser383	H-Bond	2.32
			His382	Pi-Pi stacking	5.36
		(*S*)-N4-ATTAF-2	Ser383	H-Bond	2.61
			Phe385	Pi-Pi stacking	5.08
			Phe242	Pi-Pi stacking	5.59
			Tyr141	Pi-Pi stacking	5.45
			Met512	Pi-Sulfur	4.83
3.	**3LD6**	(*R*)-N1-ATTAF-1	Thr135	H-Bond	3.16
			Tyr131	Pi-Pi stacking	4.79
			Phe234	Pi-Pi stacking	5.11
			Tyr145	Pi-Sulfur	4.80
			Phe139	Pi-Sulfur	5.51
			Phe234	Pi-Sulfur	5.60
		(*R*)-N2-ATTAF-1	Met378	H-Bond	2.81
			Val130	H-Bond	2.85
			Tyr131	Pi-Pi stacking	4.32
			Trp239	Donor-Donor (**Unfavorable**)	2.09
		(*R*)-N4-ATTAF-1	Tyr131	2 Pi-Pi stacking	4.18, 4.23
			Phe139	Pi-Pi stacking	5.14
			Tyr145	Pi-Sulfur	5.78
			Thr135	Pi-Sulfur	2.94
			Phe139	Pi-Sulfur	4.34
			Phe234	Pi-Sulfur	4.74

(*continued on next page*)

Table 4 (*continued*)

Entry	Target	Ligand	Interaction	Type of interaction	Bond distance (Å)
		(*S*)-N1-ATTAF-1	Thr135	H-Bond	1.90
			Tyr145	H-Bond	2.76
			Phe234	Pi-Pi stacking	5.23
			Tyr131	Pi-Sulfur	3.97
		(*S*)-N2-ATTAF-1	Tyr145	2 H-Bond	2.82, 3.54
			Tyr131	2 Pi-Pi stacking	4.13, 4.73
			Phe139	Pi-Pi stacking	5.09
		(*S*)-N4-ATTAF-1	Thr135	H-Bond	2.91
			Phe234	Pi-Pi stacking	5.06
			Phe234	Pi-Sulfur	5.64
		(*R*)-N1-ATTAF-2	Tyr131	H-Bond	2.53
			Thr135	H-Bond	2.64
			Tyr145	H-Bond	3.49
			Phe234	Pi-Pi stacking	4.84
		(*R*)-N2-ATTAF-2	Ile379	H-Bond	2.25
			Phe234	Pi-Sulfur	5.89
		(*R*)-N4-ATTAF-2	Tyr131	Pi-Pi stacking	4.27
			Met381	Pi-Sulfur	4.94
			Phe234	Pi-Sulfur	5.99
		(*S*)-N1-ATTAF-2	Pro379	H-Bond	2.29
			Met378	Donor-Donor (**Unfavorable**)	2.51
		(*S*)-N2-ATTAF-2	Ala311	Pi-Alkyl	4.34
			Ile379	Pi-Alkyl	4.45
			Met381	Pi-Alkyl	4.30
		(*S*)-N4-ATTAF-2	Leu310	H-Bond	2.68
			Ala311	H-Bond	2.99
			Phe234	Pi-Pi stacking	4.21

moving water molecules, ions and cocrystallized ligands, polar hydrogens addition and assigning Gasteiger-Marsili partial charges, adjusting bonds and formal charges for metals, and removing unwanted chains. In order to rmsd validation, the co-crystallized ligand was re-docked. The target input files were converted to PDBQT format for AutoDock by using the AutoDockTools-1. 5. 4.

2.2. Ligand preparation and molecular docking

Ligands 3D structures were sketched by using ChemDraw Ultra 8.0 and energy minimized using PM3 force field. For all ligands, the nonpolar hydrogen atoms were merged and the Gasteiger charges were assigned. Then set number of torsion with detect root and choose torsion in Autodock program. Later, ligand input files were also saved as PDBQT format utilizing the AutoDock Tools. The minimized structures were docked on the prepared protein.

Discovery Studio Client 2016 and Molegro Molecular Viewer were used for further analysis.

Declaration of Competing Interest

The authors declare that they have no known competing financial interests or personal relationships that could have appeared to influence the work reported in this paper.

Acknowledgments

Research reported in this publication was supported by a grant from Research Council of Mazandaran University of Medical Sciences, Sari, Iran (Grant no. 3365).

Supplementary materials

Supplementary material associated with this article can be found, in the online version, at doi:10.1016/j.dib.2020.105942.

References

[1] L. Friggeri, T.Y. Hargrove, Z. Wawrzak, F.P. Guengerich, G.I. Lepesheva, Validation of human sterol 14alpha-demethylase (CYP51) druggability: structure-guided design, synthesis, and evaluation of stoichiometric, functionally irreversible inhibitors, J. Med. Chem. 62 (22) (2019) 10391–10401 Retrieved from https://www.ncbi.nlm.nih.gov/pubmed/31663733 , doi:10.1021/acs.jmedchem.9b01485.

[2] Pooja, P. Prasher, P. Singh, K. Pawar, K.S. Vikramdeo, N. Mondal, S.S. Komath, Synthesis of amino acid appended indoles: appreciable anti-fungal activity and inhibition of ergosterol biosynthesis as their probable mode of action, Eur. J. Med. Chem. 80 (2014) 325–339 Retrieved from https://www.ncbi.nlm.nih.gov/pubmed/24794769 , doi:10.1016/j.ejmech.2014.04.063.

[3] X.L. Chang, L. Liu, N. Wang, Z.J. Chen, C. Zhang, The function of high-density lipoprotein and low-density lipoprotein in the maintenance of mouse ovarian steroid balance, Biol. Reprod. 97 (6) (2017) 862–872 Retrieved from https://www.ncbi.nlm.nih.gov/pubmed/29092018 , doi:10.1093/biolre/iox134.

[4] B.C. Monk, A.A. Sagatova, P. Hosseini, Y.N. Ruma, R.K. Wilson, M.V. Keniya, Fungal Lanosterol 14alpha-demethylase: a target for next-generation antifungal design, Biochim. Biophys. Acta Proteins Proteom. 1868 (3) (2020) 140206 Retrieved from https://www.ncbi.nlm.nih.gov/pubmed/30851431 , doi:10.1016/j.bbapap.2019.02.008.

[5] T.Y. Hargrove, L. Friggeri, Z. Wawrzak, A. Qi, W.J. Hoekstra, R.J. Schotzinger, … G.I. Lepesheva, Structural analyses of Candida albicans sterol 14alpha-demethylase complexed with azole drugs address the molecular basis of azole-mediated inhibition of fungal sterol biosynthesis, J. Biol. Chem. 292 (16) (2017) 6728–6743 Retrieved from https://www.ncbi.nlm.nih.gov/pubmed/28258218 , doi:10.1074/jbc.M117.778308.

[6] S.M. Hashemi, H. Badali, H. Irannejad, M. Shokrzadeh, S. Emami, Synthesis and biological evaluation of fluconazole analogs with triazole-modified scaffold as potent antifungal agents, Bioorg. Med. Chem. 23 (7) (2015) 1481–1491 Retrieved from https://www.ncbi.nlm.nih.gov/pubmed/25740636 , doi:10.1016/j.bmc.2015.02.011.

[7] M.V. Keniya, M. Sabherwal, R.K. Wilson, M.A. Woods, A.A. Sagatova, J.D.A. Tyndall, B.C. Monk, Crystal structures of full-length Lanosterol 14 alpha-demethylases of prominent fungal pathogens candida albicans and candida glabrata provide tools for antifungal discovery, Antimicrob. Agents Chemother. (2018), doi:10.1128/AAC.01134-18.

[8] N. Strushkevich, S.A. Usanov, H.W. Park, Structural basis of human CYP51 inhibition by antifungal azoles, J. Mol. Biol. 397 (2010) 1067–1078, doi:10.1016/j.jmb.2010.01.075.

[9] H. Irannejad, S. Emami, H. Mirzaei, S.M. Hashemi, In silico prediction of ATTAF-1 and ATTAF-2 selectivity towards human/fungal lanosterol 14α-demethylase using molecular dynamic simulation and docking approaches, IMU 20 (2020) 100366, doi:10.1016/j.imu.2020.100366.